Proc. Natl. Acad. Sci. USA
Vol. 79, pp. 1121–1125, February 1982
Biophysics

Oriented properties of the chlorophylls: Electronic absorption spectroscopy of orthorhombic pyrochlorophyllide *a*–apomyoglobin single crystals

(photosynthesis/myoglobin/protein crystal)

STEVEN G. BOXER†, ATSUO KUKI†, KAREN A. WRIGHT†, BRADLEY A. KATZ‡, AND NGUYEN H. XUONG‡

†Department of Chemistry, Stanford University, Stanford, California 94305; and ‡Department of Chemistry, University of California at San Diego, La Jolla, California 92093

Communicated by John I. Brauman, October 28, 1981

ABSTRACT **The orientations of the transition dipole moments in chlorophyll (Chl) are among the most useful spectroscopic properties for determining macromolecular architecture in photosynthetic complexes; however, the relationships between these orientations and the Chl molecular geometry are unknown. In order to solve this problem, we have prepared single crystals of the synthetic 1:1 complex between pyrochlorophyllide *a* and apomyoglobin. The protein crystallizes readily in the orthorhombic (*B*) form, space group $P2_12_12_1$, and the unit cell dimensions are determined to be within 0.5% of those for native MetMb crystals of the same type. These green crystals are highly dichroic, and the strong absorption along the crystallographic *a* axis in the Q_y band is red-shifted by about 9 nm, relative to the corresponding feature in a solution of the protein. Although the crystal structure for native Mb in this space group has not been determined, the direction cosines of the heme normal relative to the crystal axes have been measured. By using these values, an appropriate trigonometric analysis, and the measured polarized single-crystal spectra, the orientation of the Chl transition dipole moment for the Q_y transition can be specified relative to the crystal axes. With the completion of the protein crystal structure, this result will lead directly to the orientations of the optical transition dipole moments relative to the molecular geometry. The effects of vibronic coupling and the protein environment on the absorption properties of Chl are discussed in detail.**

Virtually every available spectroscopic method has been applied to study the properties of the chlorophylls (Chls) and their parent class of chromophores, the porphyrins (1). In spite of this, very little information is available on the relationship between oriented spectroscopic properties and the Chl structure (Fig. 1). Because photosynthetic reaction centers and most Chl–protein complexes thus far have eluded crystallization, spectroscopic methods provide the only means to obtain geometric information on the architecture of photosynthetic systems. In particular, spectroscopy with polarized light—for example, linear (2–4) and circular dichroism (5) or magnetophotoselection (6–8)—has been used widely. In order to translate these data from abstract relationships among vectors and magnetic axes into concrete molecular orientations, one needs to know how the transition dipole moments for the singlet excited states and principal axis system for the zero-field tensor in the lowest triplet state are oriented relative to Chl's molecular geometry. In addition, there has been a great deal of interest in the properties of Chl dimers and higher aggregates, which may be key components in the primary photosynthetic process and energy transport (5). Again, the orientation of the Q_y transition dipole moment within the monomer is essential for realistic calculations of the exciton interaction in these aggregates.

The obvious solution to this problem is to fully orient Chls as a guest in a host crystal. We have chosen to use the heme protein myoglobin (Mb), with the heme substituted by a variety of chlorophyllides, to achieve this goal (9, 10). The advantages of a protein host crystal for the spectroscopy of intrinsic chromophores was originally demonstrated in elegant studies of ferricytochrome *c* (11) and monoclinic MetMb (12) by Eaton and Hochstrasser, and studies of a variety of protein crystals have followed (13, 14). The principal requirements for success are that the chromophores under investigation be sufficiently distant from each other in the crystal to minimize interchromophore interactions, and the chromophore excited states must not interact with other intrinsic chromophores in the protein host (15). Here we demonstrate that chlorophyllide–apoMb crystals are ideal for this purpose, and obtain polarized spectra of fully oriented Chl monomers.

EXPERIMENTAL

Pyrochlorophyllide *a*–apoMb complex (PChl*a*–apoMb), ZnMb, and MgMb were prepared as described (9, 10). PChl*a* lacks the native carbomethoxy group at position 10 (Fig. 1). This derivative is used because it avoids the stereochemical ambiguity associated with epimerization at position 10 in native Chls, and, as the carbomethoxy group is not conjugated, its absence does not affect absorption in the red bands of the chromophore, either in solution or in the protein (10). Well-formed single crystals were grown from 1–2% (wt/vol) solutions of the complex in 3.14 M sodium phosphate (pH 6.8). The protein crystallizes as nearly hexagonal plates with a high dichroic ratio. Crystals for optical spectroscopy were freed from debris and sealed in the mother liquor between a coverslip and microscope slide. Absorption spectra were obtained on a home-built microspectrophotometer. The light source was a tungsten/halogen lamp, and the light was passed through a monochromater (<2-nm resolution), Glan–Thompson polarizer (extinction, $>10^{-6}$), Leitz adjustable field diaphragm, and strain-free optics. The spot size was always much smaller than the crystal, and the image was carefully optically masked to minimize artifacts from scattered light (16). Given the crystal morphology, light propagates along the *c* axis, perpendicular to the plate, and the electric vector of polarized light can be at any desired angle in the *ab* plane. It proved possible to reorient certain crystals by applying pressure to the coverslip. By this method both the thickness and OD at 675 nm could be measured for a single crystal, though with poor accuracy. Using a concentration of 0.042 M for the chro-

The publication costs of this article were defrayed in part by page charge payment. This article must therefore be hereby marked "*advertisement*" in accordance with 18 U. S. C. §1734 solely to indicate this fact.

Abbreviations: Chl, chlorophyll; PChl*a*, pyrochlorophyllide *a*; PChl*a*–apoMb, pyrochlorophyllide *a*–apomyoglobin complex.

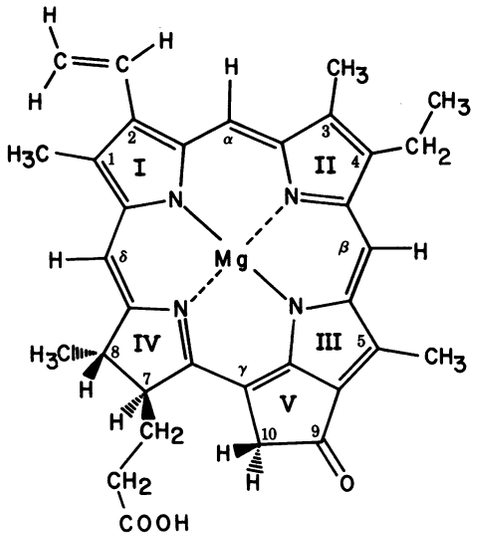

FIG. 1. Structure and numbering system for PChl*a*.

mophore in the crystal (14), we obtain $\varepsilon_{675} = 40{,}000 \pm 5000$ M^{-1} cm^{-1} for E||*a*.

A plate crystal of dimensions 0.8 mm × 0.4 mm × 0.15 mm was mounted and sealed in a glass capillary and was transferred to a multiwire area detector diffractometer at the University of California at San Diego (17). A total of 51,667 reflections to a resolution of 2.5 Å were collected using Cu/Kα radiation (λ, 1.545 Å). Lattice parameters were continually recalculated during data collection from about 100 intense reflections measured in the region of reciprocal space where data collection was occurring.

RESULTS

X-Ray Data. The crystals are orthorhombic, with space group $P2_12_12_1$ (four molecules per unit cell). The unit cell dimensions are compared in Table 1 with those reported for native orthorhombic MetMb in the classic study of Kendrew and Parrish (18) and are found to be within 0.5% of those for native MetMb. Unfortunately a complete crystal structure has not yet been obtained for this crystal form of MetMb. The normal to the heme plane was determined by Bennet *et al.* (19) from an ESR analysis of the g-tensor anisotropy for iron in orthorhombic MetMb crystals, and the direction cosines for the heme normal are included in Table 1. Roughly speaking, the macrocycle plane is perpendicular to the crystallographic *b* axis, accounting for the high dichroic ratio in both MetMb and PChl*a*–apoMb crystals.

Absorption Spectra. The absorption spectra of PChl*a*–apoMb single crystals for plane polarized light incident normal to the *ab* crystal face and with the E vector parallel to the *a* and *b* axes are compared in Fig. 2 with the solution spectrum. It is noted that the absorption maximum for the Q_y transition for E||*a* (675 nm) is red-shifted relative to that for E||*b* (666 nm) and the solution (666 nm). The wavelength dependence of the ratio of the measured OD parallel to the *a* axis [OD(*a*)] to that parallel to the *b* axis [OD(*b*)] is presented in Fig. 2 *Inset*. These ratios were obtained from data on crystals of different thickness to ensure good signal-to-noise ratios for both E||*a* and E||*b* spectra. The full angular dependence of the sample OD at 675 nm is shown in Fig. 3, and the data are compared to a calculated angular dependence of the form:

$$OD(\phi) = -\log\left[10^{-OD(a)}\cos^2\phi + 10^{-OD(b)}\sin^2\phi\right],$$

where ϕ is the angle between E and *a*. This is the angular dependence expected for an orthorhombic crystal (20, 21) and demonstrates the precision of the measurements. Orthorhombic crystals containing mesopyrochlorophyllide *a* [PChl*a* in which the vinyl group was hydrogenated (10)] and Zn-substituted PChl*a*–apoMb showed a similar red shift in the Q_y absorption maximum for E||*a* relative to solution spectra. By contrast, the absorption maxima of E||*a* for orthorhombic crystals of ZnMb and MgMb (Zn or Mg substituted for Fe) and CO–Fe(II)Mb (14) showed spectral shifts of less than 2 nm relative to solution spectra for the Soret and *Q* transitions.

Table 1. Crystallographic characteristics of orthorhombic MetMb and PChl*a*–apoMb

Unit cell dimensions, Å		Direction cosines of heme normal in MetMb†
MetMb*	PChl*a*–apoMb	
a = 48.9	a = 48.70 (4)	$\lvert z_a\rvert$ = 0.13
b = 40.2	b = 40.17 (4)	$\lvert z_b\rvert$ = 0.95
c = 79.3	c = 79.03 (7)	$\lvert z_c\rvert$ = 0.29

* From ref. 18.
† From ref. 19.

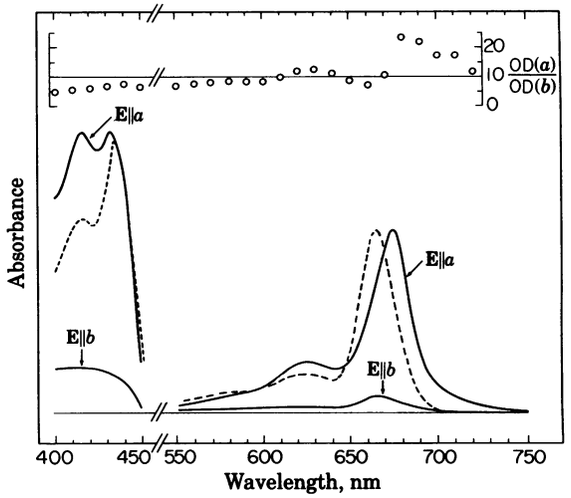

FIG. 2. Polarized absorption spectrum of PChl*a*–apoMb orthorhombic single crystals with the electric vector (E) parallel to the *a* and *b* crystallographic axes (——), compared with a solution spectrum (2.4 M sodium phosphate, pH 6.8) of the same protein (– – –). (*Inset*) Wavelength dependence of the polarization ratios [OD(*a*)/OD(*b*)].

DISCUSSION

In earlier studies of the absorption properties of single crystals of native heme proteins, the analysis was cast in terms of out-of-plane *z*-polarized vs. in-plane *xy*-polarized transitions (11, 12, 14). This is an enormous simplification and is very reasonable for heme because the π-π^* transitions are effectively degenerate in plane. This is clearly not applicable to the chlorophyllides, which are very unsymmetrical. This is precisely what makes the orientations of the transition dipole moments useful in studies of reaction center structure. A further simplification of the analysis of orthorhombic MetMb single-crystal optical data is the facile conversion of experimentally determined ODs into extinction coefficients in the crystal (14). This is accomplished by using the known extinction coefficients for solutions of the protein and the reasonable approximation that certain transitions (e.g., the Soret band) are strictly *xy*-polarized. Again, this simplification is not justified for the chlorophylls, and extinction coefficients must be determined by precise mea-

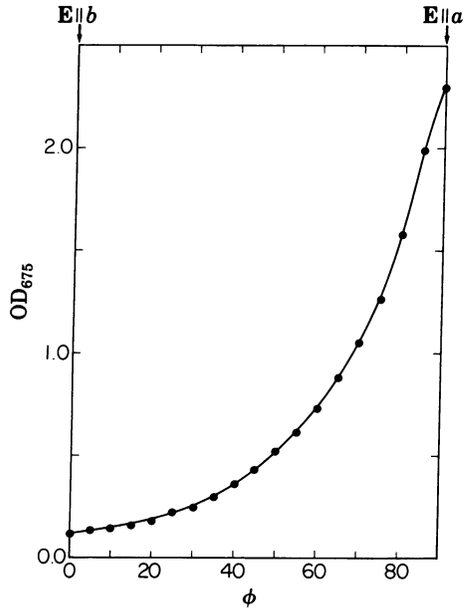

FIG. 3. Dependence of OD_{675} of an orthorhombic crystal of PChl*a*–apoMb on the angle of the electric vector of incident light relative to the *a* axis: calculated angular dependence of the OD for an orthorhombic crystal (——) and experimental data (••••••). OD(*a*) and OD(*b*) were measured to be 0.13 and 2.31, respectively, and no adjustable parameters were used. Calculated $OD(\phi) = -\log[10^{-OD(a)}\cos^2\phi + 10^{-OD(b)}\sin^2\phi]$.

surements of crystal thickness. This is a very difficult experiment and is subject to serious error, given the extremely platy habit of orthorhombic PChl*a*–apoMb. For this reason, our data reduction is in terms of polarization ratios with the light propagating along the *c* direction.

It is noted that the absorption maxima for E||*a* and E||*b* are shifted relative to each other and that the polarization ratio changes substantially across the Q_y band. The simplest explanation for this observation is that more than one electronic state is absorbing in this wavelength region. This is unlikely, based on extensive circular dichroism, magnetic circular dichroism (10), and fluorescence polarization studies (22) in solution. It is conceivable that an out-of-plane polarized transition, for example a weak $n\pi^*$ state, is detectable because of the low Q_y OD along the *b* axis. However, a number of calculations suggest that $n\pi^*$ states should be substantially higher in energy (23, 24). We can rule out resonance (exciton) interactions as the source of the shift because the chromophores are separated by at least one-half the smallest unit cell dimension (≈20 Å, Table 1). Even for the most favorable orientation of the transition dipole moments, $2(\mu^2/R^3)$ is about 24 cm^{-1}, which is much less than the observed 200-cm^{-1} shift [μ is the transition moment magnitude (25) and R is the interchromophore separation]. In the light of these comments, we consider in the following section the optical properties of orthorhombic PChl*a*–apoMb crystals in which the transition dipole moments are isolated. We will argue that this spectral shift between E||*a* and E||*b* can be understood in terms of vibronic coupling and anisotropic absorption for a single electronic transition.

Trigonometric Analysis. On the basis of extensive NMR data (10) and the extremely good agreement between the unit cell data for MetMb and PChl*a*–apoMb (Table 1), it is very reasonable to assume that the normal to the heme plane in MetMb crystals and the normal to the PChl*a* plane in PChl*a*–apoMb crystals are parallel to each other. With this assumption, we construct the coordinate system (χ,ψ,z) shown in Fig. 4: The

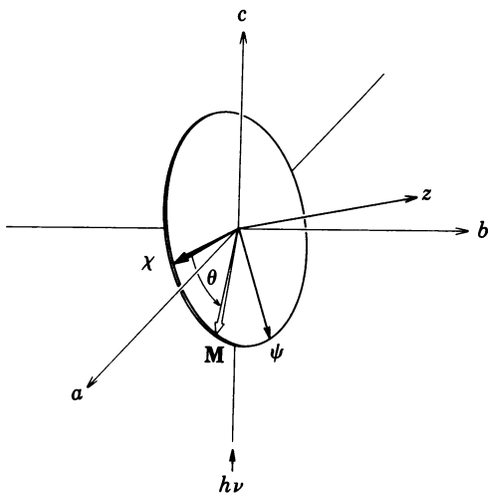

FIG. 4. Coordinate system used for the analysis of the Chl transition dipole moment orientation, **M**. *a*, *b*, and *c* are the crystallographic axes (the principal dielectric axes); the molecular axis *z* is defined as normal to the heme plane and its orientation is determined by the measured direction cosines along *a*, *b*, and *c* (Table 1); our χ molecular axis is conveniently chosen as the intersection of the *ab* and heme planes.

z axis is defined as the normal to the PChl*a* plane, with direction cosines along *a*, *b*, and *c* as given in Table 1. The orientation of the chlorin around the *z*-axis is not yet known. Thus, the conventional molecular axes labeled *x* and *y* in chlorins, to which the Chl optical transitions Q_x and Q_y are arbitrarily referred, cannot yet be specified relative to the crystallographic axes. Therefore, we conveniently *define* a χ molecular axis as the intersection of the *ab* plane and the chlorin plane. The third axis, ψ, also lies in the chlorin plane and is perpendicular to *z* and χ generating a right-hand coordinate system.

We begin with the simplifying assumption that the nondegenerate transition moment lies strictly in the chlorin plane, at some angle θ relative to the χ molecular axis. Then the transition moment vector **M** is given in terms of its components along the χ and ψ molecular axes (unit vectors $\hat{\chi}$ and $\hat{\psi}$):

$$\mathbf{M} = \hat{\chi}\cos\theta + \hat{\psi}\sin\theta. \qquad [1]$$

The ratio of OD as measured along the *a* and *b* crystallographic axes is simply the ratio of the squares of the projections of the moment along these axes (unit vectors $\hat{e}_a$ and $\hat{e}_b$):

$$\frac{OD(a)}{OD(b)} = \frac{(\hat{e}_a\cdot\mathbf{M})^2}{(\hat{e}_b\cdot\mathbf{M})^2} = \frac{[(\hat{e}_a\cdot\hat{\chi})\cos\theta + (\hat{e}_a\cdot\hat{\psi})\sin\theta]^2}{[(\hat{e}_b\cdot\hat{\chi})\cos\theta + (\hat{e}_b\cdot\hat{\psi})\sin\theta]^2}. \qquad [2]$$

Because of the symmetry, all four chromophores in the unit cell will exhibit identical polarization ratios; therefore, we can pick one and proceed. Defining the direction cosines as $z_i \equiv \hat{e}_i\cdot\hat{z}$ ($i = a,b,c$), we choose that chromophore for which z_a, z_b, and z_c are all positive and obtain:

$$\hat{e}_a\cdot\hat{\chi} = z_b(1-z_c^2)^{-1/2}; \quad \hat{e}_a\cdot\hat{\psi} = z_cz_a(1-z_c^2)^{-1/2};$$

$$\hat{e}_b\cdot\hat{\chi} = -z_a(1-z_c^2)^{-1/2}; \quad \hat{e}_b\cdot\hat{\psi} = z_cz_b(1-z_c^2)^{-1/2};$$

$$\hat{e}_c\cdot\hat{\chi} = 0; \qquad \hat{e}_c\cdot\hat{\psi} = -(1-z_c^2)^{+1/2}.$$

On insertion into Eq. 2, this gives:

$$\frac{OD(a)}{OD(b)} = \frac{z_b^2\cot\theta + z_a^2z_c^2\cot\theta + 2z_az_bz_c}{z_a^2\cot\theta + z_b^2z_c^2\cot\theta - 2z_az_bz_c}. \qquad [3]$$

Eq. 3 is plotted as a solid curve in Fig. 5 as a function of the only

unknown, the angle θ. As expected, the function is double valued because two orientations of **M** have an identical ratio of squared projections along *a* and *b*.

The generalization to the case in which **M** can have some out-of-plane *z*-component is straightforward and gives:

$$\frac{OD(a)}{OD(b)} = \frac{M_\chi^2 z_b^2 \alpha^{-1} + M_\psi^2 z_c^2 z_a^2 \alpha^{-1} + M_z^2 z_a^2 + 2M_\chi M_\psi z_a z_b z_c \alpha^{-1} + 2M_\chi M_z z_a z_b \alpha^{-1/2} + 2M_\psi M_z z_a^2 z_c \alpha^{-1/2}}{M_\chi^2 z_a^2 \alpha^{-1} + M_\psi^2 z_c^2 z_b^2 \alpha^{-1} + M_z^2 z_b^2 - 2M_\chi M_\psi z_a z_b z_c \alpha^{-1} - 2M_\chi M_z z_a z_b \alpha^{-1/2} + 2M_\psi M_z z_c z_b^2 \alpha^{-1/2}}, \quad [4]$$

where $\mathbf{M} = M_\chi \hat{\chi} + M_\psi \hat{\psi} + M_z \hat{z}$ and $\alpha \equiv 1 - z_c^2$. We do not expect the out-of-plane component of the main $\pi - \pi^*$ transitions to be very large, and plots of Eq. 4 for small fractions of out-of-plane moment (1% and 5%) are shown in Fig. 5 to illustrate their effects.

The solid curve in Fig. 5 is based entirely on the experimentally determined direction cosines of the normal to the heme plane and contains no adjustable parameters. With the reasonable assumption that PChl*a* is substituting for heme, this curve can be used to extract the angle θ for a nondegenerate PChl*a* Q_y transition moment from the polarization ratio data in Fig. 2. Because the observed polarization ratios are large, we have the pleasant coincidence that the ratio vs. θ curve is very steep; thus, small variations in the measured polarization ratio (e.g., caused by experimental error) make very little difference in the computed angle.

The observed polarization ratios across the Q_y ("0 ← 0") band vary from 6 to 24 (650–700 nm). Because it is not possible to obtain polarization data for light propagating along another principal dielectric axis, we cannot specify the out-of-plane component, M_z, and distinguish its effect from a rotation of **M** in the plane. This increases the uncertainty in the orientation of the moment; however, the effect is not very large. The value of $M_z = \pm 0.05$ is probably as large as need be considered. Thus, allowing the widest possible convolution of polarization ratio range and an M_z of ±5%, we can already restrict the transition dipole orientation to two ranges of angle: θ = 45–68° or θ = 132–176°. If, as discussed below, the variation of the polarization ratio across the Q_y ("0 ← 0") band is due to vibronic coupling, then the polarization of the long-wavelength side of the band reveals the orientation of the purely electronic transition. By using the polarization ratios from 680 nm to 695 nm and allowing $M_z = \pm 5\%$, the orientation of the pure electronic dipole then falls within the narrower range of angle: θ = 45–58° or θ = 154–176°. As explained below, consideration of the ε favors the former narrow region.

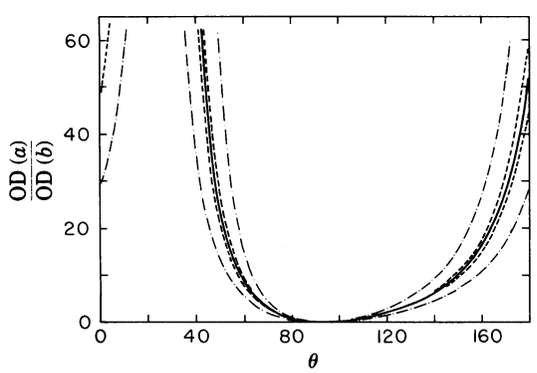

FIG. 5. Plots of Eq. 3 for $M_z = 0.00$ (——) and of Eq. 4 for $M_z = \pm 0.01$ (– – –) and ± 0.05 (·–·–·), showing the predicted values for the polarization ratios as a function of the unknown angle, θ, between the transition moment under investigation and the χ axis.

The decrease observed in the polarization ratio between 680 nm and 650 nm is a consequence of the peak shift between the **E**‖*a* and **E**‖*b* spectra. This may reflect the participation of vibronic transitions of *differing* polarization within the unresolved Q_y ("0 ← 0") envelope. Because the main pure electronic transition has a high measured polarization ratio (>20), the projection of its transition dipole onto the *b* axis must be quite small in the 650- to 670-nm region. This allows the observation in the **E**‖*b* spectrum of small contributions of different polarization, which could be vibronically induced. A quantitative analysis of the polarization ratio in the 650- to 680-nm region is complicated by the necessity to include in the treatment overlapping vibronic lines of differing orientation (i.e., degeneracy). Thus, Fig. 5, which is applicable in a vibronically resolved case to each line, cannot be used to convert ratios into angles in the vibronically unresolved 650- to 680-nm region.

Vibronic Coupling. Vibronic coupling describes the consequence of considering first-order perturbation by nuclear motion on the electronic states, which then couples an allowed transition to a forbidden one or couples two nearby allowed transitions (26). The effect of the latter case, which is important here, on the polarization of transitions was described by Albrecht (27, 28). The prerequisites of an allowed, nearby, and roughly perpendicular transition are satisfied by the Q_x band of Chl (22). The Soret bands, though more distant, are much more intense and may also contribute. In vibronically resolved crystal spectra of molecules with higher symmetry, individual vibronic lines can appear in one polarized spectrum and essentially vanish for the other polarization (29). PChl*a* has lower symmetry, and the spectrum is unresolved; thus, we are left with "mixed polarization" (30). The effect of the nearby Q_x transition on the Q_y ("1 ← 0") vibronic band (at 620 nm) is evident in fluorescence polarization experiments on Chl (22). Indeed, the polarization ratio we observe at 620 nm is different from that at 680 nm. We suggest that vibronic coupling also can explain the difference in band shapes for **E**‖*a* and **E**‖*b* spectra and the changing polarization ratio in the 650- to 680-nm region. The unusual sensitivity of the measurements reported in this paper to small vibronic components is simply the result of the particular orientation of PChl*a* in this crystal form of PChl*a*–apoMb.

It is interesting to contrast the case of orthorhombic PChl*a*–apoMb with that of MetMb, containing either Fe, Zn, or Mg as the central metal. Because of the higher symmetry of the porphyrin, the *Q* bands are best described as planar oscillators; consequently, effects based on differing orientations of the transition moment in the plane are not expected. In fact, we observe no difference between the peak maxima in their polarized spectra, which is fully consistent with the vibronic interpretation of the PChl*a*–apoMb crystal spectra.

The Unobserved E‖*c* Spectrum. Further quantitative analysis is handicapped by the lack of experimental data for **E**‖*c* or an "isotropic" crystal spectrum. If this data were available, we would know whether the protein crystal environment causes the spectral shift seen for **E**‖*a* relative to solution. Though we cannot directly measure the peak position and relative intensity of the **E**‖*c* spectrum, we can deduce approximate values for both as follows. The ε for a random isotropic set of chromophores is equal to the average of the three orthogonal projections of an oriented set. The ε of PChl*a*–apoMb in solution is about 5.7×10^4 M^{-1} cm^{-1} (10) and triple this value is about 171,000.

Because ε_{675} was measured to be about 40,000 ± 5000 $M^{-1}cm^{-1}$ for E||*a*, over 120,000 is left unaccounted for and must be contained in the unobservable E||*c* spectrum. The total peak ε may change upon crystallization (e.g., the band may broaden); nevertheless, the conclusion remains that the greater part of the total transition intensity partitions into the unobserved E||*c* spectrum.

We now consider and reject an argument that the peak position of this E||*c* spectrum may be shifted with respect to that of E||*a* through anisotropic absorption in the manner of the small E||*b* peak. Shpolskii single-site fluorescence excitation spectra of Chl*a* and chlorin have established that the vibronic transitions of these molecules in the Q_y ("0 ← 0") region are much weaker than the intense pure electronic origin (31, 32). It follows that neither the large E||*a* or the larger E||*c* spectrum can be dominated by vibronic contributions because the total vibronic contribution in the Q_y ("0 ← 0") band is small. Thus, both the E||*a* and E||*c* spectra are expected to exhibit peak maxima very close to that of the pure electronic origin; the former is at about 675 nm, as discussed above.

Because the visible absorption spectrum of PChl*a*–apoMb in solution is indistinguishable from that of PChl*a* in organic solvents (9), it is surprising that crystallization has an impact on the absorption spectrum. The dielectric properties in the immediate vicinity of the chromophore should not change. It is possible that the coordination number of the central metal changes when the protein is crystallized. In all reported cases, Zn-containing porphyrins are five coordinate (32), and because Zn- and MgPChl*a*–apoMb crystals both show the same spectral shift, a change in coordination number is an unlikely mechanism to produce the shift. It is possible that the vinyl group at position 2 (Fig. 1) is rotated out of plane in the crystal but not in solution. The equivalent vinyl group in monoclinic crystals of MetMb is rotated substantially out of the heme plane (34). However, the same spectral shift is observed when the vinyl group is removed from conjugation by hydrogenation to an ethyl group. Furthermore, ZnMb and MgMb, which contain the native vinyl groups at positions 2 and 4, show no spectral shift. In fact, the validity of the "oriented gas approximation" has been extensively tested and confirmed for a wide variety of liganded hemes in Mb in the identical space group (14). Thus, a remaining possibility is that the protein, upon crystallization, interacts differently with the five-membered exocyclic ring V than it does in solution. Possible interactions are hydrogen bonding to the carbonyl group in ring V (conceivably to Arg-CD3) or electrostatic interactions with neighboring charged groups (a negative charge in the vicinity of the carbonyl group is predicted to cause a substantial red shift; J. Eccles and B. Honig, personal communication). The former proposal could be tested by resonance Raman spectroscopy and the latter with model compounds.

Finally, we have analyzed the angular dependence of OD(*c*)/OD(*a*) (derived exactly as Eq. 3). The calculated OD(*c*)/OD(*a*) values for the pure electronic transition in the θ = 45–58° region range from 1.0 to 2.2. This range is consistent with the independent ε considerations above. On the other hand, the calculated OD(*c*)/OD(*a*) values from the θ = 154–176° region range from 0.23 to 0.005, leading to an unrealistically small average ε of 20,000 or less for the Q_y band. For this reason, we consider this range of angle to be a poor choice and favor θ = 45–58° as the orientation of the Q_y electronic transition moment.

In summary, we have provided spectroscopic data for chlorophyll monomers fully oriented in three dimensions and an outline of a method of data analysis that yields the orientation of the transition dipole moment for the Q_y band relative to the crystallographic axes. With the completion of the protein crystal structure, these results will lead directly to the long-desired orientation of the optical transition dipole moment relative to the molecular geometry. The orthorhombic unit cell is also ideal for studying the fully oriented ESR spectra of the lowest triplet excited state and of the radical cation and anion.

We thank Prof. Makinen for excellent advice on the construction and use of a microspectrophotometer. This work is supported by National Science Foundation Grant PCM 79-26677, U.S. Department of Agriculture Science and Education Administration Grant 78-59-2066-0-1-147-1, and Department of Energy Grant DE-FG02-80-CS84006. S.G.B. is an Alfred P. Sloan and Camille and Henry Dreyfus Teacher-Scholar Fellow.

1. Dolphin, D., ed. (1979) *The Porphyrins* (Academic, New York), Vol. 3–5.
2. Vermeglio, A., Breton, J., Paoillotin, G. & Cogdell, R. (1978) *Biochim. Biophys. Acta* **501**, 514–530.
3. Rafferty, C. N. & Clayton, R. K. (1979) *Biochim. Biophys. Acta* **546**, 189–206.
4. Shuvalov, V. A. & Asadov, A. A. (1979) *Biochim. Biophys. Acta* **545**, 296–308.
5. Sauer, K. (1975) in *Bioenergetics of Photosynthesis*, ed. Govindjee (Academic, New York), pp. 115–181.
6. Thurnauer, M. C. & Norris, J. R. (1977) *Chem. Phys. Lett.* **47**, 100–105.
7. Boxer, S. G. & Roelofs, M. G. (1979) *Proc. Natl. Acad. Sci. USA* **76**, 5636–5640.
8. Frank, H. A., Bolt, J., Friesner, R. & Sauer, K. (1979) *Biochim. Biophys. Acta* **547**, 502–511.
9. Boxer, S. G. & Wright, K. A. (1979) *J. Am. Chem. Soc.* **101**, 6791–6794.
10. Wright, K. A. & Boxer, S. G. (1981) *Biochemistry* **20**, 7546–7556.
11. Eaton, W. A. & Hochstrasser, R. M. (1967) *J. Chem. Phys.* **46**, 2533–2539.
12. Eaton, W. A. & Hochstrasser, R. M. (1968) *J. Chem. Phys.* **49**, 985–995.
13. Eaton, W. A., Hofrichter, J., Makinen, M. W., Andersen, R. D. & Ludwig, M. L. (1975) *Biochemistry* **14**, 2146–2151.
14. Churg, A. K. & Makinen, M. W. (1978) *J. Chem. Phys.* **68**, 1913–1925.
15. Rohleder, J. W. & Luty, T. (1968) *Mol. Crystals* **5**, 145–163.
16. Howling, D. H. & Fitzgerald, P. J. (1959) *Biophys. Biochem. Cytol.* **68**, 313–337.
17. Cork, C., Fehr, D., Hamlin, R., Vernon, W., Xuong, N. H. & Perez-Mendez, V. (1974) *J. Appl. Crystallogr.* **7**, 319–323.
18. Kendrew, J. C. & Parrish, R. G. (1956) *Proc. R. Soc. London Ser. A* **238**, 305–324.
19. Bennet, J. E., Gibson, J. F., Ingram, D. J. E., Houghton, T. H., Kerkut, G. A. & Munday, K. A. (1961) *Proc. R. Soc. London Ser A* **262**, 395–408.
20. Albrecht, A. C. & Simpson, W. T. (1955) *J. Chem. Phys.* **23**, 1480–1485.
21. Eaton, W. A. & Lewis, T. P. (1970) *J. Chem. Phys.* **53**, 2164–2172.
22. Gouterman, M. & Stryer, L. (1962) *J. Chem. Phys.* **37**, 2260–2266.
23. Weiss, C. (1972) *J. Mol. Spectro.* **44**, 37–80.
24. Spangler, D., Maggiora, G. M., Shipman, L. & Christoffersen, R. E. (1977) *J. Am. Chem. Soc.* **99**, 7478–7489.
25. Shipman, L. (1977) *Photochem. Photobiol.* **26**, 287–297.
26. Herzberg, G. & Teller, E. (1933) *Z. Phys. B* **21**, 410–446.
27. Albrecht, A. C. (1960) *J. Chem. Phys.* **33**, 156–169.
28. Albrecht, A. C. (1961) *J. Mol. Spectro.* **6**, 84–108.
29. Hochstrasser, R. M. & Small, G. J. (1966) *J. Chem. Phys.* **45**, 2270–2284.
30. Albrecht, A. C. (1960) *J. Am. Chem. Soc.* **82**, 3813–3816.
31. Platenkamp, R. J., den Blanken, H. J. & Hoff, A. J. (1980) *Chem. Phys. Lett.* **76**, 35–41.
32. Volker, S. & Macfarlane, R. M. (1980) *J. Chem. Phys.* **73**, 4476–4482.
33. Hoard, J. L. (1975) in *Porphyrins and Metalloporphyrins*, ed. Smith, K. M. (Elsevier, New York), p. 345.
34. Kendrew, J. C. (1962) *Brookhaven Symp. Biol.* **15**, 216–227.